U-(Th)-Pb systematics and mineralogy of single crystals and concentrates of accessory minerals from the Cacciola granite, central Gotthard massif, Switzerland

Autor(en): **Oberli, F. / Sommerauer, J. / Steiger, R.H.**

Objekttyp: **Article**

Zeitschrift: **Schweizerische mineralogische und petrographische Mitteilungen = Bulletin suisse de minéralogie et pétrographie**

Band (Jahr): **61 (1981)**

Heft 2-3

PDF erstellt am: **21.07.2024**

Persistenter Link: https://doi.org/10.5169/seals-47144

Schweiz. mineral. petrogr. Mitt. 61, 323–348, 1981

U-(Th)-Pb systematics and mineralogy of single crystals and concentrates of accessory minerals from the Cacciola granite, central Gotthard massif, Switzerland

by *F. Oberli**, *J. Sommerauer** and *R. H. Steiger**

Abstract

U-Pb isotopic analyses and electron microprobe studies have been carried out on sieve fractions of accessory zircon as well as on single grains of zircon and monazite separated from the Cacciola granite. Together with the Rotondo and Winterhorn granite this leucogranite forms part of the younger group of Variscan granites in the central Gotthard massif. The zircons show unusually high U concentrations (> 1 wt.%) and are intimately intergrown with allanite, epidote and less frequently with apatite containing minute inclusions of Th-U phases. Isotope analyses of individual grains disclose distinct U-Pb isotopic patterns which are averaged out when concentrates consisting of large numbers of grains are investigated by conventional methods. Using refined analytical techniques a relatively precise age of 292 ± 9 m.y. was obtained and interpreted as the time of intrusion for the Cacciola granite.

Acid-leaching experiments on the samples reveal a highly selective response of their U-Th-Pb systems to external processes. This is a consequence of the complex textural relationship between the zircons and the coexisting less resistant Th and U rich phases.

1. Introduction

The present study is part of a program to investigate U-Th-Pb systematics of accessory minerals by microanalytical techniques. The purpose of this program is to gain insight into petrogenetic processes and to solve geochronological problems by detailed isotopic studies on a grain-by-grain basis. This approach has been used for the analysis of extraterrestrial matter (TERA and WASSERBURG, 1975; WASSERBURG et al., 1977) and has been successfully applied to terrestrial samples, in particular for the study of complex zircon populations (LANCELOT et al., 1976; MICHARD-VITRAC et al., 1977; LUDWIG and STUCKLESS, 1978). It has become possible to identify zircon grains recording different source ages within

* Institute of Crystallography and Petrography, Federal Institute of Technology, CH-8092 Zurich, Switzerland.

single rocks (GAUDETTE et al., 1981; SCHÄRER and ALLÈGRE, 1981a). Domains with widely differing U-Pb characteristics have been identified within individual zircon grains suggesting highly specific response of individual domains to external processes (GRÜNENFELDER, 1963; SOMMERAUER, 1974; KROGH and DAVIS, 1975; SCHÄRER and ALLÈGRE, 1981b).

Analytical limitations set by the minimum quantities of radiogenic Pb required for precise U-Pb analysis have confined application of these techniques predominantly to zircon populations of Precambrian origin. The present study extends the applications to an investigation of U-Pb systematics in zircons and monazite from a granite of Variscan age. During preliminary examination, the zircon concentrate of the Cacciola granite in the central Gotthard massif was found to contain unusually large amounts of uranium. The zircons thus appeared suitable for a detailed U-Pb isotopic study, in particular for a comparison of conventional methods with grain-by-grain analytical techniques. In view of the highly radioactive nature of the minerals it was also of interest to examine the stability of their U-Pb system. To test this point all samples were subjected to acid-leaching experiments before dissolution. From the resulting isotopic patterns conclusions can be drawn with respect to the stability of the accessory minerals in the actual geological environment.

The complex morphological and textural properties of the minerals analyzed as well as the isotopic results obtained called for a quantitative mineralogical and chemical characterization of the samples. A study of polished grains by electron microprobe was therefore carried out providing important clues for the interpretation of U-Pb isotopic data.

Structural studies in the central Gotthard massif suggest the existence of two intrusive cycles during the Variscan orogeny. The original geochronological work by GRÜNENFELDER (1962), GRÜNENFELDER and HAFNER (1962), JÄGER and NIGGLI (1964) and JÄGER (1979), however, does not allow to resolve the sequence of emplacement for the Variscan granites unequivocally. In this work we present data using refined analytical techniques which improve the resolution of isotopic age determination. It will be of interest to see whether this method will eventually enable us to establish the sequence of these intrusions on an absolute basis.

2. The Cacciola granite

2.1 Geologic setting

The Gotthard massif – by some investigators believed to represent the front of a lower Penninic nappe (TRÜMPY, 1980) – consists of three major elongated zones of basement which parallel the overall eastnortheasterly trend of the massif (Fig. 1).

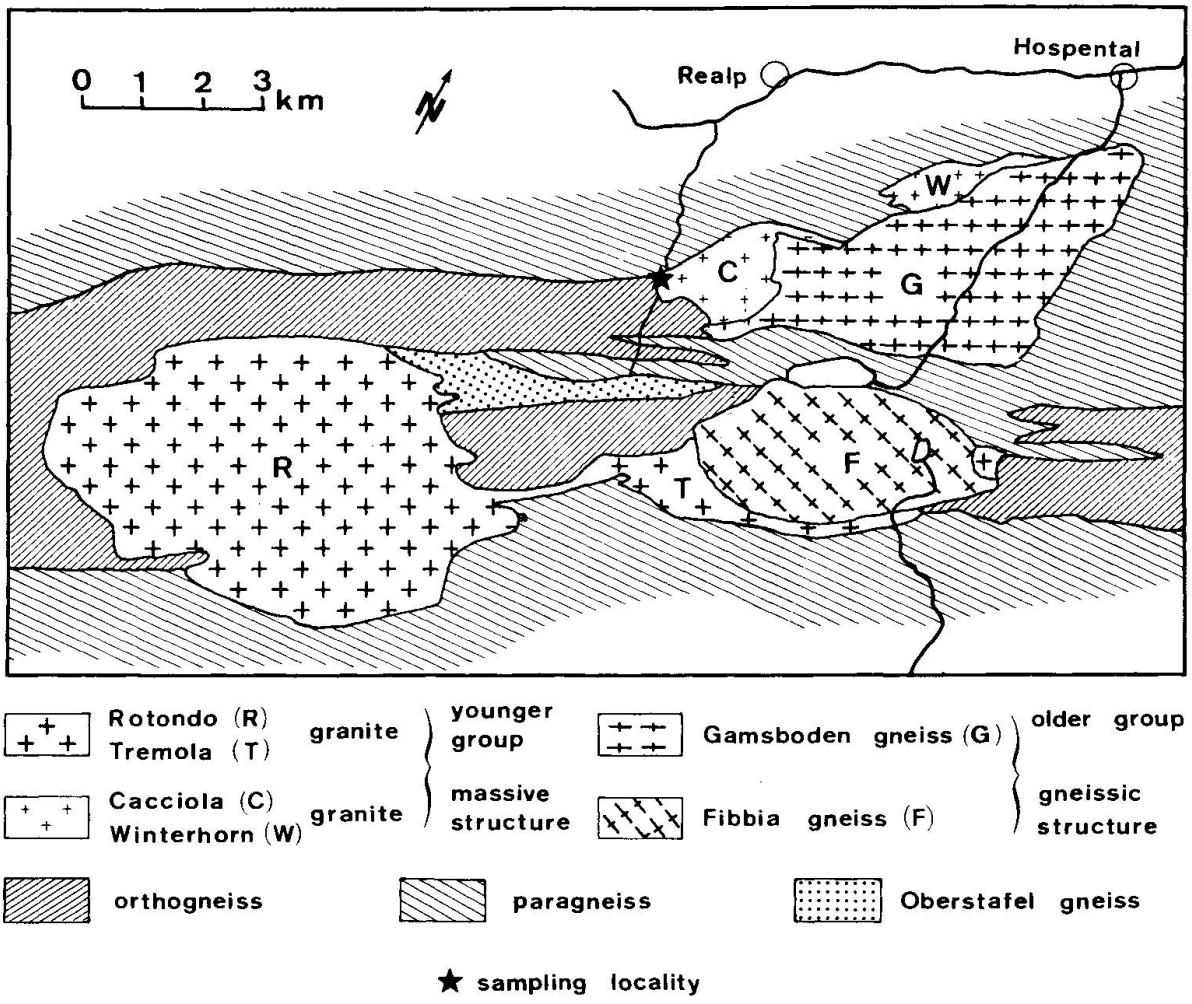

Fig. 1 Synoptic geologic map of the central Gotthard massif (after HOFMÄNNER, 1964). Prominent are the Variscan granites: an older group with gneissic structure partially mantled by massive granites of the younger group. Both groups are accumulated in or along the margin of the orthogneiss-dominated central zone of the massif.

The *Cacciola granite*, situated between the northern paragneiss zone and the complex central orthogneiss zone, is spatially associated with the *Winterhorn granite*. Together they form part of the NW margin of the *Gamsboden* pluton, much in analogy with the *Tremola* granite which embraces the *Fibbia* stock from the SSE and which lies between the southern paragneiss and the central zone. All the granitoid plutons mentioned clearly cut through the structural trend and schistosity of the basement zones of the massif.

On the basis of their structure and petrofabric the granitoid intrusives of the central Gotthard massif are subdivided into two groups:

1) the Gamsboden and Fibbia stocks, coarse-grained porphyritic *gneisses* with phenocrysts or porphyroblasts of K-feldspar,
2) the Cacciola / Winterhorn granites and the Rotondo / Tremola granite, displaying a massive equigranular medium- to fine-grained structure.

It appears that the Gamsboden and Fibbia plutons were emplaced earlier and suffered some deformation whereas the Rotondo/Tremola- and the Cacciola/Winterhorn granites intruded after this deformative phase. For this reason, we distinguish an older and a younger group of granitoids in Fig. 1. It was AMBÜHL (1929), who first suggested this sequence of events. This age relation is supported by the fact that both the Rotondo and the Cacciola granites contain gneissic xenoliths similar to the Fibbia and Gamsboden gneisses (HAFNER, 1958; HOFMÄNNER, 1964).

2.2 Petrography

With respect to chemical composition the granites within each group are closely related and both groups show calc-alcalic affinity. The magma of the older group belongs to the yosemitic type, that of the younger group to the aplite granitic type (SONDER, 1921; HOFMÄNNER, 1964). This led to the concept that all granitoid stocks in the central Gotthard massif derive from a deep-seated magma complex which successively generated rock types of increasingly aplitic composition (SONDER, 1921).

Hardly any difference is recognized in the modal composition within each group. The main constituents of the Cacciola granite (HOFMÄNNER, 1964) are quartz (24–40%), plagioclase of An_{0-4} (25–35%) and perthitic alkali-feldspar (microcline, 25–35%). Biotite (0.5–6%) and white mica (1–3%) represent minor constituents. The accessories (0–3%) are epidote, garnet, apatite and zircon. However, HOFMÄNNER's (1964) study did not prepare for the unusually high radioactivity encountered in these accessory minerals. The few radiometric measurements actually made on rock samples of the Cacciola granite indicated concentrations of radioelements varying from 12 to 20 ppm eU with an average of only about 15 ppm eU, a value comparable to those of the neighboring Gamsboden and Fibbia stocks (HOFMÄNNER, 1964; RYBACH and HAFNER, 1962). The analyses by HOFMÄNNER (1964) possibly indicate some inhomogeneity but no obvious zonation pattern for the distribution of the radioactive elements within the Cacciola pluton.

While the texture of the Cacciola granite is subhedral-granular, typical of a granite, a minor metamorphic overprint is recognized on the basis of partially fractured and recrystallized quartz and from alteration of plagioclase to secondary white-mica and epidote. This apparent low-grade overprint of the Cacciola granite is compatible with values of 450 °C and 3 kbars assumed for the climax of Alpine metamorphism in the area (FREY et al., 1980). Age determinations by JÄGER and NIGGLI (1964), JÄGER (1979), on the Rotondo granite and by JÄGER et al. (1967) on the Fibbia and Gamsboden gneisses suggest that the Rb-Sr mineral ages were indeed reset during the Tertiary.

2.3 Previous age determinations

On geologic grounds the intrusion of the gneissic Gamsboden and Fibbia plutons was assumed to have taken place in pre-Triassic times (HEIM, 1921, p. 191), presumably during the Variscan (Hercynian) orogeny. This was confirmed by GRÜNENFELDER (1962) who obtained $^{207}Pb/^{206}Pb$ ages of 280 ± 50 m.y. on zircon concentrates separated from the Gamsboden stock and 370 ± 60 m.y. for the Fibbia stock (ages recalculated with the JAFFEY et al., 1971, U decay constants). However, the age of intrusion for the granites of the younger group, in particular that of the Rotondo granite and its eastern off-shoot, the Tremola granite, has been much debated during the past century. The dearth of gneissic structure and of Alpine lineation in these rocks was used as an argument for a late Alpine age of intrusion (KVALE, 1957; HAFNER, 1958), whereas opponents pointed to the scarcity of micaceous component and the lack of Variscan planar structure in these granites impeding the formation of readily recognizable Alpine lineation (SONDER, 1921; JÄGER and NIGGLI, 1964). While the zircon age work by GRÜNENFELDER and HAFNER (1962) did not yield an unequivocal result (170 ± 70 m.y.), the controversy around the Rotondo granite was ultimately settled by the Rb/Sr whole-rock isochron age of 272 m.y. (recalculated with new constants) obtained by JÄGER and NIGGLI (1964). This age, later revised to 269 ± 11 m.y. (JÄGER, 1979), definitely assigned the granites of the younger group to the Variscan cycle. Up to now, no isotopic age has been determined for the Cacciola granite proper.

The granite sample used for the present study was collected by drilling and blasting from a fresh occurrence at the western margin of the Cacciola pluton (Fig. 1). The sample is from the only outcrop on the western side of the Witenwasserenreuss stream. The collection site is near Sunnsbiel (coordinates 681.25/157.50) at an altitude of 2050 m.[1])

3. Mineralogy of the accessory minerals

The zircon concentrate of the Cacciola granite revealed several uncommon features which called for closer inspection. Particularly striking were the high radioactivity recognized during preliminary alpha-counting and the unusual appearance of the minerals.

---

[1]) It is interesting to note in this context that HAFNER, who mapped the pertinent part of the «Val Bedretto» sheet of the Swiss Geological Atlas (HAFNER et al., 1975), attributed the sampling locality to the Rotondo granite, whereas in the theses of SONDER (1921) and of HOFMÄNNER (1964) the site is clearly assigned to the Cacciola granite.

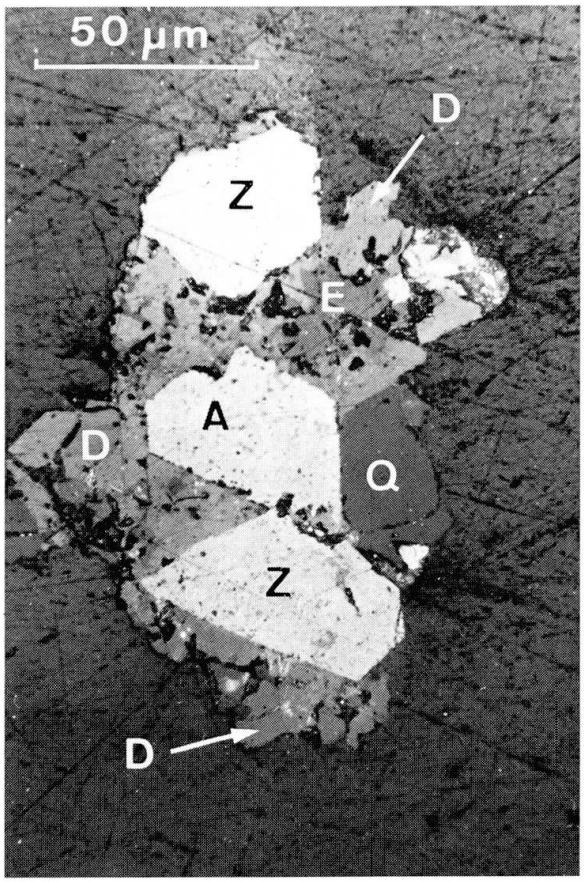

Fig. 2a

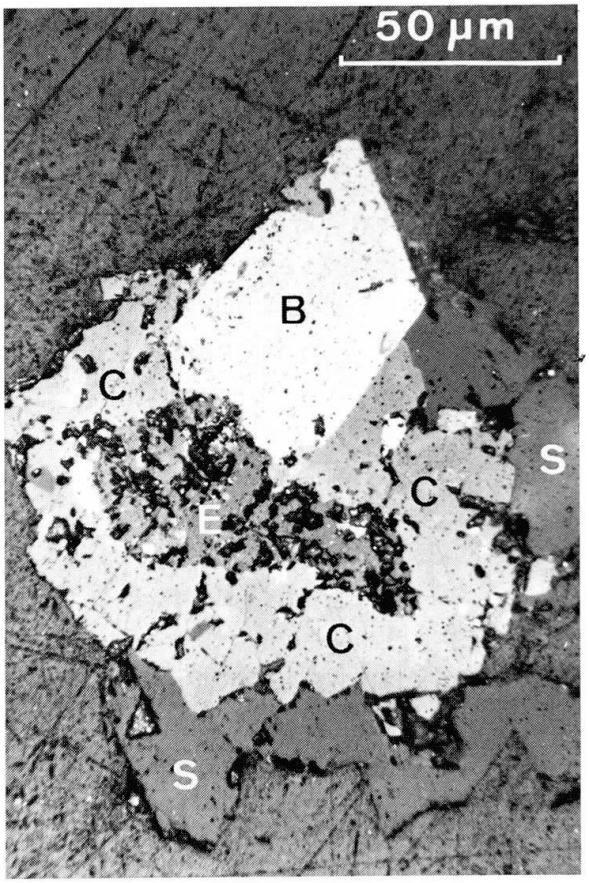

Fig. 2b

Figures 2a and 2b Reflected light micrographs of polished sections showing representative intergrowth textures of zircon aggregates typically found in the > 120 µm «zircon» fraction of the Cacciola granite. The aggregates are embedded in epoxy resin. The mineral phases forming part of the assemblage are labelled as follows: *A*:zircon crystal in Fig. 2a (analyses A in Table 1); *B*:zircon crystal in Fig. 2b (analyses B in Table 1); *C*:irregular grain of the allanite-epidote series in Fig. 2b (analyses C in Table 2); *D:* phases from the allanite-epidote series in Fig. 2a (analyses D in Table 2); *E:* grain of apatite with submicroscopic inclusions (in some of the dark spots) presumably of thorianite and thorite; *Q:* quartz grain; *S:* silicates (Fig. 2b), mainly albite; *Z:* zircon crystals having the same compositional range as zircon A. In reflected light allanite cannot be distinguished from epidote. The most conspicuous feature: the euhedral zircon crystals (A, B, Z) are mantled by or intergrown with allanite-epidote, apatite and silicates.

3.1 Textural relations and morphology

The study of polished sections showed that the zircon suite from the western margin of the pluton is unique both in morphology and texture. It is distinct from the zircon population of the adjacent Rotondo granite (GRÜNENFELDER and HAFNER, 1962) and from the zircons of the Cacciola granite investigated by HOFMÄNNER (1964). Fig. 2 depicts representative views of polished grains which are recognized to be aggregates of zircon crystals intimately intergrown with other mineral phases.

The zircon crystals are overgrown by allanite, epidote, apatite, quartz and feldspars. Th-U phases occur predominantly as minute inclusions in apatite.

The zircons are generally euhedral, forming short prismatic crystals. In contact with epidote and allanite they occasionally show resorption features (Fig. 2a). The zircons are usually mantled by allanite and epidote, less frequently by other silicate phases. In contrast to the zircons all other coexisting phases are anhedral. In reflected light the zircons reveal small patches of lower reflectivity (Fig. 2a, grains A and Z). These are quite distinct from the numerous tiny inclusions present in the zircon crystals.

In view of the complex mineralogical texture of these samples the distribution of the radioactive elements uranium and thorium and the physico-chemical stability of their host phases is of fundamental interest for the interpretation of the U-Th-Pb isotopic data.

3.2 Mineral chemistry

Analytical procedure

Zircon and other phases were investigated using an automated ARL SEMQ microprobe equipped with an X-ray energy dispersive analyzer (TN 2000 by Tracor Northern). Five crystal X-ray spectrometers and the X-ray energy dispersive system were applied simultaneously for quantitative analyses. An acceleration potential of 15 KV with a sample current of 20 nA (measured on brass) was applied yielding a beam size of 0.2 μm. For X-ray energy data collection integration time including dead-time was 40 seconds per analysis resulting in counting statistics better than 0.3% (1 sigma) for the minor and major elements. Natural and synthetic oxides, silicates and phosphates were used as standard materials (SOMMERAUER, 1976). The samples as well as the standards were coated with 200 Å of carbon. On-line corrections for drift, dead-time and background were applied to the raw data. Full correction for X-ray absorption, atomic number effect and X-ray fluorescence (by characteristic and continuum excitation) were based on a ZAF program for the CDC Cyber-720 computer system at the ETH Zurich.

Zircons

Elemental abundances (wt.%) including means and standard deviations as well as pertinent chemical ratios and correlation coefficients are compiled in Table 1. The data reflect the distinct chemical heterogeneities of zircons of magmatic origin (GRÜNENFELDER, 1963; KÖPPEL and SOMMERAUER, 1974). Note that the variation in elemental abundances are not primarily caused by the visible inclusions present in many of the zircon crystals. They relate to zircon domains of microscopic to submicroscopic size which often can be distinguished optically. These domains also reveal varying cathodoluminescence (C.L.) response. Domains enriched in minor elements substituting for Si and Zr (Table 1, see correlation coefficient $\gamma_{(Zr\text{-}«Zr»)}$ and $\gamma_{(Si\text{-}«Si»)}$) exhibit low C.L. intensity whereas those depleted in these constituents show high C.L. intensity (SOMMERAUER,

Table 1 Representative electron microprobe analyses showing: the compositional range of zircon grain A in Fig. 2a; means and standard deviation for zircon A as well as zircon B (Fig. 2b) and, for comparison, results of a zircon from the Gneiss Chiari; oxide ratios and correlation coefficients (γ) for some pertinent components. Besides the elements listed, traces of Ti, Mg, Mn, and Al up to 0.1 wt.% each have been determined.

	A/32	A/33	A/34	A/35	A/36	A/37	A mean 6 analyses	B mean 8 analyses	Gneiss Chiari[1] 25 analyses
ZrO_2	55.7	57.0	60.5	64.2	59.7	58.6	59.28 ± 2.98	58.7 ± 3.9	60.48 ± 3.82
SiO_2	30.5	29.5	30.7	31.3	31.6	30.4	30.67 ± 0.74	30.3 ± 2.5	29.87 ± 1.99
HfO_2	2.43	2.0	1.87	1.98	1.94	1.86	2.01 ± 0.21	2.12 ± 0.13	2.07 ± 0.73
Y_2O_3	1.69	2.49	1.64	0.41	1.14	1.98	1.55 ± 0.70	1.99 ± 2.17	0.84 ± 0.55
UO_2	5.38	3.36	1.80	1.14	1.65	2.22	2.59 ± 1.56	4.04 ± 3.16	0.70 ± 0.60
ThO_2	0.65	0.20	<0.05	0.34	<0.05	0.16	0.23 ± 0.24	0.32 ± 0.30	0.07 ± 0.07
Fe_2O_3	0.50	0.02	0.36	<0.03	0.28	0.13	0.22 ± 0.20	0.26 ± 0.23	0.65 ± 0.54
CaO	0.06	0.43	0.19	0.14	0.13	0.07	0.17 ± 0.14	0.18 ± 0.35	0.48 ± 0.48
P_2O_5	0.69	1.60	0.98	<0.04	0.26	1.34	0.81 ± 0.62	1.04 ± 1.74	0.90 ± 0.80
Σ *)	97.60	96.60	98.04	99.51	96.70	96.76	97.52	98.95	96.06
Cations normalized to 4 oxygens, see note 2)									
Zr	0.884	0.902	0.934	0.981	0.930	0.916	0.925	0.913	0.950
Hf	0.022	0.018	0.016	0.017	0.017	0.017	0.018	0.019	0.018
Y	0.029	0.043	0.027	0.006	0.019	0.033	0.026	0.033	0.014
U	0.039	0.024	0.012	0.008	0.011	0.015	0.018	0.028	0.005
Th	0.004	0.001	0.000	0.002	0.000	0.001	0.001	0.002	0.000
Fe	0.012	0.000	0.008	0.000	0.006	0.003	0.005	0.006	0.015
Ca	0.002	0.015	0.006	0.004	0.004	0.002	0.005	0.006	0.016
	0.994	1.005	1.007	1.020	0.990	0.989	0.985	1.010	1.022
Si	0.993	0.957	0.972	0.981	1.009	0.975	0.981	0.967	0.963
P	0.019	0.044	0.026	0.001	0.007	0.036	0.022	0.028	0.024
	1.012	1.001	0.998	0.982	1.016	1.011	1.003	0.995	0.987

Sample	ZrO_2/SiO_2	$\gamma_{(Zr\text{-}Si)}$[3]	$\gamma_{(Zr\text{-}"Zr")}$[4]	$\gamma_{(Si\text{-}"Si")}$[5]	Y_2O_3/P_2O_5	$\gamma_{(Y\text{-}P)}$[6]	ThO_2/UO_2	$\gamma_{(U\text{-}Th)}$[7]
A	1.93 ± 0.08	0.63	-0.91	-0.91	1.91	0.96	0.09	0.74
B	1.94 ± 0.09	0.87	-0.93	-0.92	1.91	1.0	0.08	-0.19
Chiari	2.02 ± 0.08	0.87	-0.95	-0.94	0.93	0.66	0.10	0.40

Notes: 1) leucocratic gneiss, Valle Colla zone, Southern Alps (Sommerauer, 1976); 2) water (molecular and OH) has not been taken into account, compare Sommerauer (1976); 3) correlation coefficient for ZrO_2 and SiO_2; 4) c. coeff. for ZrO_2 and the sum of substituting elements; 5) c. coeff. for SiO_2 and the substituting elements; 6) c. coeff. for Y_2O_3 and P_2O_5; 7) c. coeff. for UO_2 and ThO_2; *) tot. H_2O content may be approximated by difference, see also note 2)

1974). As has been demonstrated by SOMMERAUER (1976) these domains of differing C.L. response show distinctly different susceptibility to metamictization and thus have different physico-chemical stability. It is important to note that the domains are not forming any zonation pattern.

The chemical abundances and heterogeneity as well as the distribution pattern of the domains are comparable with those observed in the highly metamict zircons from the gneiss Chiari in the Southern Alps (KÖPPEL and GRÜNENFELDER, 1971; KÖPPEL and SOMMERAUER, 1974). However, the zircons from the Cacciola granite show substantially higher concentrations of uranium. On the other hand, the gneiss Chiari zircons appear to contain more H_2O as inferred from the significantly lower Σ of the chemical constituents (Table 1).

The ThO_2/UO_2 ratios found in the Cacciola granite zircons (Table 1) are as low as would be expected for accessory zircons (SOMMERAUER, 1976), but there exists no obvious correlation (Table 1, $\gamma_{(U\text{-}Th)}$) between the uranium and thorium contents. Of the coexisting phases in the intergrowth texture zircon is the main U-bearing phase. Thus it is the zircons which govern the U-Pb isotopic pattern of the mineral assemblage.

Mineral phases coexisting with the zircons

Allanite and epidote, intimately intergrown with the zircons (Fig. 2) do not form separate phases. In contrary, the variable amounts of cerium, lanthanum and thorium obviously substituting for calcium suggest a series between epidote and allanite (Table 2, analyses C/3 to C/15). Analyses D/39 and D/41 are distinct from analyses C/3 to C/15, in particular with respect to Th, U and P contents. In analysis D/41 ThO_2 attains close to 40 wt.%. By optical means, however, locations D/39 and D/41 could not be resolved as separate phases. From the data it is evident that allanite is the major Th-bearing mineral phase of the intergrowth assemblage.

Monazite was detected as a separate phase not forming part of the zircon-allanite-apatite intergrowth texture. Whereas Th was found uniformly distributed within some individual grains, the grain-to-grain variation is rather large (about 1–20 wt.% Th).

Apatite is abundant in the intergrowth texture (Fig. 2b), however, the mineral proper contains only trace amounts of the radioactive elements.

Xenotime was not observed.

Th-U phases of submicroscopic scale, occasionally containing Si, occur as inclusions within the apatite (Fig. 2b). Because of small size no quantitative electron microprobe analysis could be carried out. Based on the X-ray energy dispersive spectra these phases nonetheless may be interpreted as $(Th, U)O_2$

Table 2 Electron microprobe analyses of the allanite-epidote series of sample C (Fig. 2b) and sample D (Fig. 2a).

	C/3	C/4	C/5	C/14	C/15	D/39	D/41
SiO_2	37.3	32.1	31.5	38.1	34.5	24.5	18.7
Al_2O_3	24.6	18.2	17.0	24.8	19.5	10.2	4.20
Fe_2O_3	9.81	13.5	16.0	10.1	12.2	7.70	3.00
CaO	20.6	12.2	10.8	20.5	16.2	7.90	2.90
ThO_2	1.09	1.02	0.42	<0.05	0.36	22.2	37.3
UO_2	0.82	0.81	<0.05	0.25	0.62	5.50	23.5
Y_2O_3	1.47	0.26	0.41	1.53	0.39	0.88	2.50
Ce_2O_3	0.65	9.10	9.30	0.58	5.09	6.83	1.50
La_2O_3 [1]	0.50	9.40	10.4	0.60	6.90	7.60	1.20
P_2O_5	<0.04	0.04	0.04	0.04	0.04	2.28	2.00
H_2O [2]	2.0	2.0	2.0	2.0	2.0	2.0	2.0
tot [3]	96.84	96.59	95.83	96.66	95.76	95.59	96.80
Number of cations on the basis of 13 (O+OH)							
Si	3.020	2.927	2.909	3.056	3.017	2.725	2.611
Al	2.347	1.956	1.851	2.344	2.010	1.337	0.689
P	<0.004	<0.004	<0.004	<0.004	<0.004	0.215	0.236
Fe	0.598	0.926	1.112	0.610	0.803	0.644	0.315
Ca	1.787	1.192	1.069	1.762	1.518	0.941	0.434
Th	0.020	0.021	0.009	<0.001	0.007	0.562	1.185
U	0.015	0.016	<0.001	0.004	0.012	0.136	0.730
Y	0.063	0.013	0.020	0.065	0.018	0.052	0.186
Ce	0.019	0.304	0.315	0.017	0.163	0.278	0.077
La	0.015	0.316	0.354	0.018	0.223	0.317	0.062
OH	1.080	1.216	1.232	1.070	1.167	1.484	1.863

Notes: 1) Other rare earth elements may be present but were not analyzed
2) H_2O has been approximated by a fixed value and may not be appropriate for precise stoichiometry
3) The total does not include the assumed H_2O concentration of 2 wt.%

(thorianite) and (Th, U)SiO_4 (huttonite or thorite). Thus apatite as host of these inclusions must also be considered an important contributor to the U-Th-Pb isotopic data pattern.

4. U-Pb isotope analysis: Experimental Procedures

4.1 Mineral preparation

The heavy mineral concentrate was extracted from some 160 kg of fresh rock by standard techniques: crushing and grinding of the material to particle size < 300 μm, density separation using a Wilfley table, tribromomethane and methylene iodide. After removal of minerals of high magnetic susceptibility by means of a Frantz Isodynamic Separator a grain concentrate of 4.1 g, rich in zircon but containing other radioactive minerals as well, was obtained. By sieving, this concentrate was divided into several size fractions. Sample C-1 represents a split from size fraction 58–75 μm and sample C-2 is a split of the most «magnetic» sub-fraction from size fraction < 30 μm (Table 3). These two zircon splits were carefully handpicked before isotopic analysis in order to remove any detectable non-zircon grains. For single-grain analysis one grain each of zircon (sample C-3) and monazite (sample C-A) were selected from size fraction > 120 μm. From this fraction we also picked the grains used for the electron microprobe study. Up to this stage of preparation, the samples had been in contact with water and organic liquids only and were not exposed to any of the acid treatments usually applied during zircon separation.

4.2 Acid-leaching experiments and extraction of U and Pb

In order to remove residual contamination from the mineral separation procedure, all samples were soaked at room temperature in a solution consisting of 94% CH_3OH and 6% HNO_3 conc. (by volume) for 30–40 minutes and rinsed with H_2O. These wash and rinse solutions were discarded. The samples were then leached for 30–45 minutes in 0.4–0.6 ml 4.7 N HCl while the temperature was gradually increased from room temperature to about 80 °C. The leach solutions were transferred with a quartz pipette into separate beakers. The solid leached samples as well as the leach solutions were spiked with a mixed ^{205}Pb-^{235}U tracer and evaporated to dryness. The tracer contains 400 ng ^{235}U and 0.95 ng ^{205}Pb per gram of solution with ^{205}Pb enriched to 99.3%. Decomposition of the solid samples and extraction of U and Pb were done using the methods developed by KROGH (1973); reagents and column volumes, however, were reduced by a factor of 2.5. Column yields for U and Pb amounted to 90%.

Pb and U in the wash solution of single grain samples C-3 and C-A were measured without further purification. An attempt to apply this technique also to the highly concentrated leach solution L-1 of sample C-1 resulted in the loss of the Pb run on the mass spectrometer. Therefore, a small amount of this sample left from filament loading as well as the total leach of sample C-2 were purified using the same ion exchange procedure as for the solid samples. The fraction of Pb from leach solution L-1 left for purification was 2.9% as determined in a separate yield experiment. This large reduction of sample size led to a considerable amplification of the blank corrections as seen from the data in Table 4 and Fig. 3.

4.3 Blanks

All reagents used were purified by surface distillation at subboiling temperatures. H_2O (1.8 pg Pb/g) (1 pg = 10^{-12} g) was prepared in a quartz still, HCl (16 pg Pb/g), HF (2.5 pg Pb/g) and HNO_3 (9.3 pg Pb/g) by the two-bottle still technique of MATTINSON (1972). The nominal total Pb blank used for correction of the data from the leached solid samples (S) amounts to 72 pg and is the sum of the blanks for hydrothermal decomposition (40 pg), ion exchange column (29 pg) and filament loading (3 pg). Its composition was $^{208}Pb/^{204}Pb$ = 37.23, $^{207}Pb/^{204}Pb$ = 15.40, $^{206}Pb/^{204}Pb$ = 17.66. Proof of stable blank conditions was obtained by the analysis of a single 2.55 b.y. old zircon grain from an East Greenland basement rock simultaneously processed with the present samples. A total amount of 73 pg common Pb was measured in this grain, in excellent agreement with the blank data reported here. For the leach analyses L-3 and L-A, total blanks were 6.6 pg and 7.1 pg ($^{208}Pb/^{204}Pb$ = 37.8, $^{207}Pb/^{204}Pb$ = 16.4, $^{206}Pb/^{204}Pb$ = 18.2) and 33 pg for L-1 and L-2 ($^{208}Pb/^{204}Pb$ = 37.73, $^{207}Pb/^{204}Pb$ = 15.68, $^{206}Pb/^{204}Pb$ = 18.16), respectively. Since U blanks were < 2 pg, no blank corrections were applied to U measurements.

4.4 Mass spectrometry

The isotopic measurements were carried out on a Varian MAT Tandem mass spectrometer (GRAUERT et al., 1973; GEBAUER and GRÜNENFELDER, 1974) connected to an RTE operated computer system model 1000 of Hewlett-Packard for on-line data acquisition and reduction (OBERLI, 1976). Lead was run on outgassed single rhenium filaments with standard H_3PO_4-silicagel emitter at temperatures $\geqq$ 1350 °C in order to assure contamination-free Pb spectra. Major isotopes ^{208}Pb, ^{207}Pb and ^{206}Pb of sample S-1 and single zircon sample S-3 were run on a Faraday collector (10^{11} Ω resistor), the rest of the Pb measurements using a secondary electron-multiplier. For the U measurements on samples S-1 to S-A a graphite loading technique (CHEN and WASSERBURG, 1981) was adopted; poor U beam intensities obtained on our machine required use of the multiplier. The U and Pb fractions from the leach solutions were loaded on the same filament, following the procedure for Pb described above. After collection of sufficient Pb data the temperature of the filament was increased to approximately 1600 °C, and U was measured as UO_2^+ on the multiplier. All U and Pb isotopic ratios determined with the multiplier were adjusted by a factor equal to the square-root of the mass ratios in order to correct for the ion beam-to-electron yield conversion bias of the multiplier. Furthermore, all measured isotopic ratios (higher mass in the numerator) were corrected for vaporisation fractionation by the following factors (per mass unit) determined from repeat standard runs: 1.0007 (Pb), 0.998 (U, graphite load), 1.001 (U, H_3PO_4-silicagel load).

4.5 Analytical uncertainties

The overall analytical uncertainties given in Table 4 correspond approximately to the 95% confidence level. The correlated errors shown are based on Gaussian error propagation comprising the precision of the mean ratios of the individual mass spectrometer run, an uncertainty of ± 0.05% p.m.u. for Pb mass fractionation correction, a "standard" uncertainty of ± 0.5% for U mass fractionation correction and uncertainties of Pb

blank corrections. On the basis of repeat blank experiments, the latter are assessed to be twice the nominal blank given in section 4.3 as an upper limit and half the nominal blank as a lower limit for analyses S-1 to S-A. For all leach analyses (L), the corresponding values are equal to twice and 0.8 times the nominal blank, respectively.

For low amounts of Pb, where Pb blank uncertainties dominate the analytical error, asymmetric errors may result. Where differences between lower and upper error limits exceeded 10%, both limits are shown in Table 4. Since the asymmetries did not significantly alter the age results, asymmetric error limits were averaged for the graphical presentation of the data in Fig. 3 as well as for the calculation of linear-fit and age parameters. The error figures shown in Fig. 3 are 95% probability ellipses (BURINGTON and MAY, 1970, p. 129f).

5. Results and Discussion

5.1 U-Pb analytical data

The U-Pb analytical data are shown in Tables 3 and 4 and are plotted in Fig. 3. Age data are based on constants recommended by the IUGS Subcommission on Geochronology (STEIGER and JÄGER, 1977). The label *S* in the first column of the tables and in Fig. 3 designates data from the acid-leached samples, whereas *L* refers to data obtained on the corresponding acid-leach solutions. For each sample, the analytical data of the solid samples and leach fractions have been combined to yield the U-Pb data representative of the original state *C* of the samples before acid-leaching. Depending on sample size and mineralogical differences, the quantities of U and Pb available for analysis vary widely (Table 4, columns 2–6).

Observed values of $^{206}Pb/^{204}Pb$ (Table 4, column 7) show considerable spread. $^{206}Pb/^{204}Pb$ in the leached solid samples ranges from 236 to 2918. There is no correlation with sample weight (Table 3) among the three zircon fractions as would be expected if this variation were dominated by the presence of common Pb from analytical sources. On the contrary, single zircon sample S-3 having the lowest sample weight (11.2 μg) yielded the highest *measured* value for $^{206}Pb/^{204}Pb$, indicating good control of analytical blank. The total amount of ^{204}Pb measured in sample S-3 corresponds to 97 pg total common Pb if all ^{204}Pb were introduced by analytical contamination. The nominal analytical blank correction (72 pg Pb) applied to this sample leaves a residual of only 25 pg common Pb, increasing the $^{206}Pb/^{204}Pb$ ratio to 11000. Conversely, rather low $^{206}Pb/^{204}Pb$ values have been measured for grain-size fractions S-1 and S-2. Due to the relatively large amount of common Pb contained in these samples, correction for analytical blank merely increases the $^{206}Pb/^{204}Pb$ ratio from 741 to 746 for sample S-1 and from 367 to 373 for sample S-2. A similar pattern is also observed for the leach fractions of all four samples analyzed.

Uranium, total Pb and common Pb concentration data are shown in Table 3. Since Th has not been mesured, the apparent Th/U ratios listed in column 8

Table 3 Sample description. U-(Th)-Pb concentrations.

Sample[a]	Type[b]	Size[c] μm	Weight Analyzed μg	U ppm[d]	Total Pb ppm[d]	Common Pb ppm[d]	Th/U[e]
Zircon							
S - 1	F	58-75	530	11700	203	17.2	0.131
L - 1				943	58.8	44.5	2.65
C - 1				12600	262	61.7	0.237
S - 2	F	<30[f]	100	13300	250	39.8	0.144
L - 2				1210	86.0	46.2	7.76
C - 2				14500	336	85.9	0.561
S - 3	S	200/120	11.2[g]	11300	398	2.3	0.222
L - 3				1210	22.3	3.3	1.46
C - 3				12500	420	5.7	0.264
Monazite							
S - A	S	270/170	17.3[g]	857	261	4.4	27.2
L - A				1140	70.8	13.9	13.2
C - A				2000	331	18.3	23.1

a) S: acid-leached sample; L: acid-leach fraction; C: total sample

b) F: sieve fraction; S: single grain

c) Size range of sieve fraction; max. length/width dimensions for single grains

d) With respect to weight before acid-leaching; corrected for analytical blank

e) Apparent weight ratio derived from $^{208}Pb_{rad}/^{206}Pb_{rad}$ (see text)

f) Most magnetic sub-fraction

g) Maximal weight calculated from grain dimensions assuming a density of 4.0 for (metamict) zircon and 5.2 for monazite.

have been calculated from the $^{208}Pb_{rad}/^{206}Pb_{rad}$ ratios given in Table 4 (see Appendix II).

The uranium concentrations of the three zircon samples (C-1, C-2 and C-3) are extremely high, ranging from 12500 ppm to 14500 ppm and conform well to the results obtained by microprobe analysis (Table 1). Despite the gross difference in physical properties of the zircon fractions analyzed, the uniformity of these U concentrations is remarkable.

Due to the high U (and Th) contents of the samples the Pb contained in the three zircon samples and in the monazite sample is predominantly radiogenic. Common Pb contents, however, vary among the three zircon samples. Whereas single-zircon grain C-3 has a low content of common Pb (1.3% of total Pb), rather high values of 24% and 26% were measured for grain-size fractions C-1 and C-2 respectively. The common Pb content of the monazite sample (C-A) is intermediate at 5.5%.

Substantial amounts of U and Pb are located in grain sites which are readily attacked by the acid-leaching procedure. Inspection of the U data obtained from the acid-leach solutions of the zircon samples shows that approximately 10% of the total U have been extracted by the acid treatment. In the case of the monazite sample containing 2000 ppm U more than 50% have been removed. In the leach fractions common Pb is enriched with respect to the leached samples. The acid-leach solutions of the zircon grain-size fractions C-1 and C-2 are dominated by common Pb, whereas Pb leached from single-grain sample C-3 is still fairly radiogenic. Potential sources of U and Pb found in the leach solutions are

(i) mineral phases other than zircon such as the mineral phases forming the intergrowth (Fig. 2) in the coarse grain-size fractions studied by electron microprobe
(ii) distinct U-bearing inclusions in zircon
(iii) zircon phases and domains prone to metamictization and thus susceptible to leaching.

While contributions from sources (ii) and (iii) cannot be excluded due to the fact that single-grain sample C-3 contributed a similar percentage of U as size-fraction samples C-1 and C-2, other dominant contributors have to be identified among the minerals forming the intergrowth. Allanite and apatite with its inclusions of Th-U phases carry appreciable amounts of Th and U and thus of radiogenic Pb, as well as trace amounts of common Pb. Principle sources for common Pb attached to the zircon grains are feldspar and ore particles. Despite the careful preparation of zircon fractions C-1 and C-2 by hand-picking under a binocular microscope, the non-specific morphological properties of the Cacciola zircon population greatly reduced our ability to recognize

Table 4 U-Pb analytical data: absolute amounts and isotopic ratios.

Sample	Moles x 10^{-12} corrected for analytical blank					Observed[a]	Corrected for blank and common lead[b]			
	^{238}U	^{208}Pb	^{207}Pb	^{206}Pb	^{204}Pb	$\frac{^{206}Pb}{^{204}Pb}$	$^{206}Pb/^{238}U$	$^{207}Pb/^{235}U$	$^{207}Pb/^{206}Pb$	$^{208}Pb/^{206}Pb$
Zircons										
S - 1	25781	41.60	31.95	448.5	0.6009	740.6	0.01697± 9	0.1206± 7	0.05154± 14	0.04249± 22
L - 1	2085	76.01	25.31	47.67	1.5536	30.09	0.00920±12	0.0661±107	0.05211±821	0.8603 ±150
C - 1	27866	117.61	57.26	496.2	2.155		0.01639± 9	0.1165± 11	0.05157± 36	0.07685± 81
S - 2	5533	14.383	8.939	97.78	0.2621	366.5	0.01680± 9	0.1206± 10	0.05204± 31	0.04673± 74
L - 2	503.9	25.19	5.020	10.954	0.3042	35.88	0.01067± 9	0.0713± 43	0.04846±287	2.518 ± 31
C - 2	6037	39.58	13.959	108.73	0.5663		0.01629± 8	0.1165± 10	0.05184± 32	0.1819 $^{+15}_{-12}$
S - 3	529.5	1.4408	1.0230	19.135	0.001717	2918	0.03608±19	0.2594± 16	0.05215$^{+14}_{-12}$	0.07198$^{+45}_{-32}$
L - 3	56.38	0.4132	0.07212	0.7194	0.002460	250.4	0.01196±12	0.0822$^{+20}_{-25}$	0.04987$^{+106}_{-140}$	0.4730 ± 33
C - 3	585.9	1.8539	1.0951	19.854	0.004177		0.03376±18	0.2424± 15	0.05207$^{+15}_{-12}$	0.08566$^{+56}_{-34}$
Monazite										
S - A	61.87	19.249	0.19225	2.255	0.005029	236.4	0.03495±21	0.2531$^{+60}_{-33}$	0.05252$^{+106}_{-57}$	8.812 $^{+22}_{-31}$
L - A	82.57	4.412	0.2924	1.1776	0.01580	72.88	0.01076±13	0.0756± 31	0.05095±188	4.286 ± 17
C - A	144.44	23.66	0.4847	3.432	0.02083		0.02112±16	0.1516$^{+31}_{-23}$	0.05206$^{+93}_{-66}$	7.495 $^{+15}_{-19}$

a) Corrected for spike contribution

b) Numbers following ± sign correspond to total analytical error (95 % confidence level) and refer to last digits of corresponding ratios. Where uncertainties are asymmetric, both upper and lower error bounds are shown.

non-zircon grains in the finer grain-size fractions. In contrast to the hundreds and thousands of grains which had to be examined by the handpicking procedure, single grains such as sample C-3 with distinctly better morphology and surface purity, can readily be selected with minimum effort, if analytical techniques are adequate for processing of small samples.

5.2 Age of crystallization and metamorphism

In order to obtain age information, the radiogenic Pb component has to be determined by subtraction of the common Pb component from the total Pb measured in the samples. This correction requires knowledge of the appropriate isotopic composition of the common Pb phase indigenous to the samples. A discussion of the Pb composition used for the common Pb correction is given in Appendix I. U/Pb ratios, $^{207}Pb/^{206}Pb$ and $^{208}Pb/^{206}Pb$ ratios corrected for common Pb are presented in Table 4, columns 8–11.

The data are plotted in a $^{206}Pb/^{238}U$ vs. $^{207}Pb/^{235}U$ concordia diagram (Fig. 3). With the exception of the data points for leach fractions L-1 and L-2, all data points are discordant, i.e. they lie distinctly off the concordia curve. On the other hand, all data points fall on or very close to the straight line (discordia) shown in Fig. 3, which is the best-fit line (WILLIAMSON, 1968) for the four data points C-1, C-2, C-3 and C-A. We note that these four points lie precisely (see insert of Fig. 3) on the best-fit line, which intersects the concordia curve at 292 ± 9 and 11 ± 9 m.y. The uncertainties associated with the ages were determined from the intersections of the error envelopes (not shown) of the best-fit line with the concordia curve (LUDWIG, 1980).

The perfect linear relationship of the four samples leads to the conclusion that they crystallized at the same time and therefore are cogenetic. The time of crystallization is then defined by the upper intersection with concordia at 292 m.y. From this we conclude that the Cacciola granite formed during the Variscan cycle approximately at the Permian/Carboniferous boundary (ARMSTRONG, 1978). The absence of inherited Pre-Variscan Pb component in the samples favors a magmatic origin of the granite.

The age of 292 m.y. conforms with the range of the previously reported Variscan ages for the other granitic bodies in the vicinity of the Cacciola granite. The 269 ± 11 m.y. Rb/Sr whole-rock isochron age of the Rotondo granite reported by JÄGER (1979) is somewhat younger than the zircon age of the Cacciola granite. The existence of data points (JÄGER and NIGGLI, 1964) which plot below this isochron has been interpreted by JÄGER (1979) to reflect local opening of Rb/Sr whole-rock systems during Alpine metamorphism. It is therefore not clear whether the apparent difference between the zircon age of the Cacciola granite and the Rb-Sr age of the Rotondo granite marks a real time difference

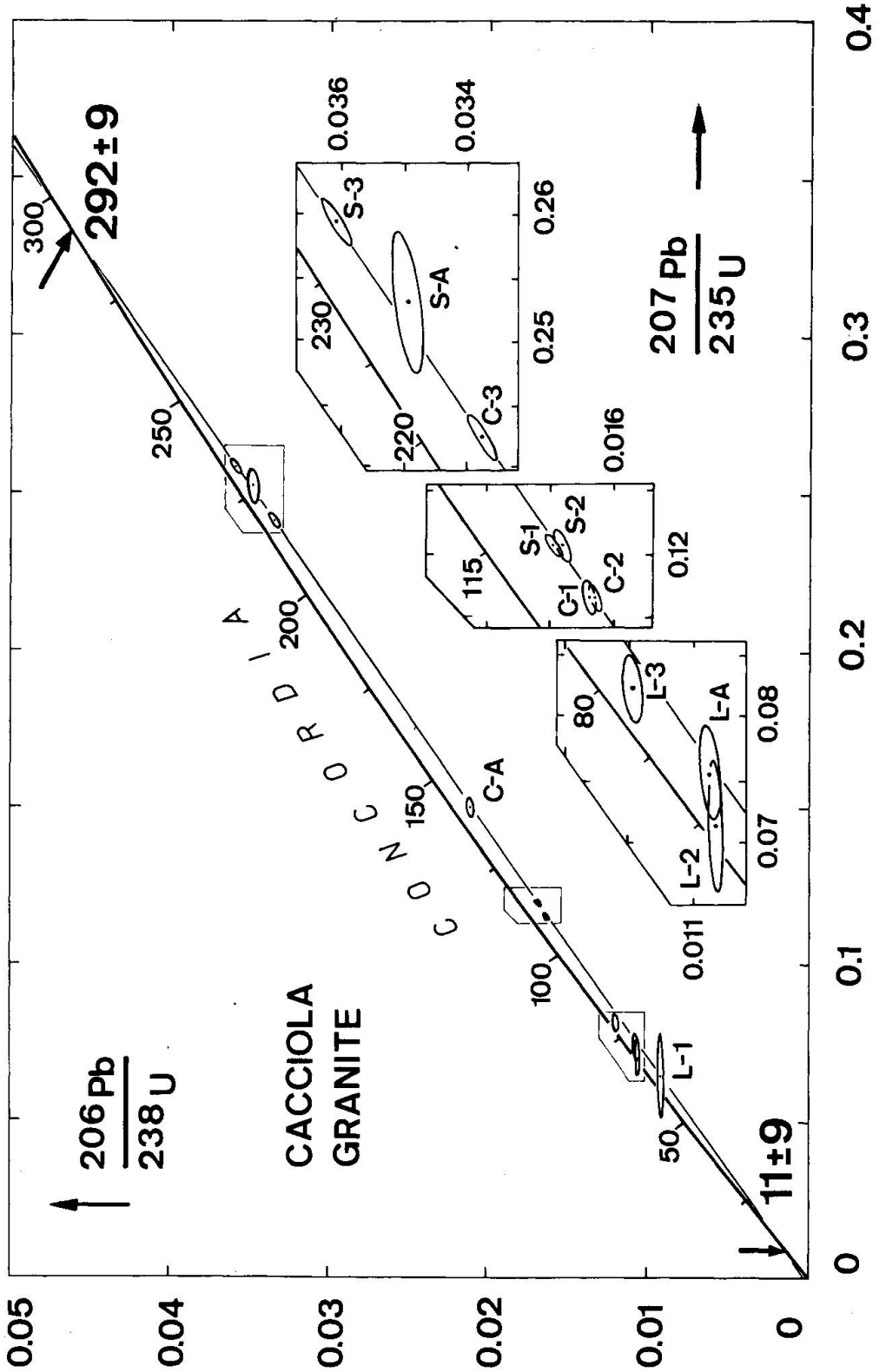

Fig. 3 Conventional concordia diagram. Age marks on the curve labelled «Concordia» are given in units of 10^6 years before present. U-Pb data of zircon grain size fractions 1 (58–75 µm), 2 (< 30 µm, most magnetic fraction), a single zircon grain (3) and a single monazite grain (A) are shown. The letters *S*, *L* and *C* refer to the data points of the acid-leached solid samples (*S*), the acid-leach solution (*L*) and the total samples (*C*) (calculated by combining the data from analyses *S* and *L*). All data are corrected for common Pb and blank Pb (see text). The best-fit line based on data points C-1, C-2, C-3 and C-A intersects the concordia curve at 292 ± 9 m.y. and 11 ± 9 m.y. Selected areas of the graph are shown in inserts, which have identical enlargement factors. The error ellipses correspond to the 95% confidence level.

for the intrusions or whether it is the result of a disturbance of the Rb-Sr system of the Rotondo granite. Due to analytical limitations, the earlier U-Pb data obtained by GRÜNENFELDER and HAFNER (1962) from a zircon sample of the Rotondo granite were interpreted by these authors in terms of a minimum crystallization age of approximately 140 m.y. Data on zircons from the older group of granites also gave Pb/Pb ages of Variscan affinity: $^{207}Pb/^{206}Pb$ ages were 280 ± 50 m.y. for the Gamsboden gneiss and 370 ± 60 m.y. (recalculated with the JAFFEY et al. 1971, U decay constants) for the Fibbia gneiss (GRÜNENFELDER, 1962). Due to lack of modern high quality age data the sequence of emplacement of the various Variscan granites remains yet to be determined.

The fact that the data points of the three zircon samples and the monazite grain plot at different positions on the best-fit line below the upper intercept indicates that these minerals were open to loss of radiogenic Pb and/or gain of U at times significantly later than the time of original crystallization. The absence of a zonation pattern (see section 3.2) leads to the conclusion that loss of radiogenic Pb and not U gain is the dominant cause of the observed U-Pb discordance. In terms of an episodic model (WETHERILL, 1956) the linear array of data points in Fig. 3 is thus the result of Pb loss induced by an event occurring at a time defined by the 11 ± 9 m.y. lower intersection of the best-fit line with concordia. This time interval coincides with a late phase of Alpine metamorphism which led to local homogenization of Sr isotopes (STEIGER and BUCHER, 1978). It appears that this phase can also be recognized in the Rb-Sr mineral isochron of the Rotondo granite obtained by JÄGER (1979), which yields 15.0 ± 0.6 m.y. Pb loss induced by pressure relief (GOLDICH and MUDREY, 1972) and interaction with fluids during an uplift phase active for the last 19 m.y. in the Gotthard region (WAGNER et al., 1977) may have enhanced the discordance of the U-Pb systems of the samples.

Besides episodic models for loss of radiogenic Pb, long-term diffusion processes could also have contributed to the observed data pattern, in particular, when the high contents of radioelements are taken into account. Direct application of the basic models of continuous diffusion (TILTON, 1960; WASSERBURG, 1963) does not yield a satisfactory fit to all data points. The model by STEIGER and WASSERBURG (1969, Fig. 1e and 1f) based on continuous diffusion but taking into account the observed heterogeneity of the zircons, possibly offers a better explanation for the present case. These authors suggested that natural zircons might essentially be viewed as binary mixtures of concordant phases and highly discordant phases, a finding supported by the crystalchemical evidence presented by SOMMERAUER (1976). Depending on the degree of discordance chosen for the highly discordant phase (possibly represented by the leach-solutions) straight-lines can be generated which will fit any data array with a slope equal to or steeper than that of the linear region of the corresponding continuous diffusion trajectory. It is obvious that in this case the lower intersection of the best-fit line with the concordia curve has no time significance.

We conclude that none of the processes discussed above can be considered a unique solution for the cause of discordance. It is most likely that all have contributed to a certain degree to the U-Pb systematics observed, but there is little doubt that the Alpine metamorphism has played an important part in it.

5.3 The pattern of discordance: mineralogical aspects

The following trends emerge from the pattern of the data points in Fig. 3:

In both zircon and monazite analyses the acid-leaching procedure leads to fractional loss of U and Pb resulting in the displacement of the data points for solid samples (S) with respect to those of the untreated samples C-1 to C-A. In each case the leach-fractions (L) are more discordant than the untreated samples (C), which causes the data points of the leached samples S to be displaced towards the upper intercept, i.e. to become more concordant. For the data point of the single monazite grain, the displacement is substantial. From the highly discordant position of the data point C-A, the data point of the acid-leached sample S-A shifts to a position close to the most concordant zircon data point S-3.

The limited spread of the data from the acid-leach solutions (L-1 to L-A) suggests that the mineral assemblage attacked by the leaching procedure may be rather similar for all four samples. In view of the dominance of the Th-derived lead component ^{208}Pb in the leach fractions the sources for this Pb are most likely phases such as allanite and the various Th-U phases included within apatite which are intergrown with the zircon crystals (see Appendix II). The displacement of the data points for the leach fractions in the direction of the lower intercept in Fig. 3 suggests that the phases leached had lost considerably more radiogenic Pb during their history than the more resistant phases surviving the acid-leaching procedure. Similar observations have been made by STEIGER and WASSERBURG (1969) in their study of zircons from 2.7 b.y. old granitic plutons.

The fact that the highly discordant phases are so easily removed under laboratory conditions – causing the remaining samples to become more concordant – suggests that such an effect could also be achieved in the environment of progressive metamorphism. A scenario can be conceived where progressive metamorphism leads to dissolution of metamict minerals or domains of minerals which had lost radiogenic Pb already at earlier stages. If conditions are not favorable for in situ recrystallization of dissolved U and Th bearing matter, the initial trend to increase discordance will then be reversed, due to net loss of U and Th. Increasingly more concordant systems will be generated, as long as the threshold conditions for release of radiogenic daughter elements from the more retentive mineral sites are not exceeded. The argument presented here may at

least partially explain the lack of correlation between discordance and degree of metamorphism often observed for zircon suites.

It is rather surprising that the data points obtained from the zircon grain-size fraction 58–75 μm (C-1) and from the finest (< 30 μm) most magnetic zircon fraction (C-2) plot on the same position on the discordia line, as do the data points of the acid-leached zircon fractions (S-1 and S-2). These data points with minimal spread are derived from zircon concentrates separated by conventional techniques.

The key to explain the close similarity between the isotopic systems of samples C-1 and C-2 and their dissimilarity with the isotopic system of sample C-3 lies most likely in the variability of structural state and in the chemical heterogeneities of individual zircon grains detected by the electron microprobe (Table 1). The analysis of zircon fractions consisting of hundreds or thousands of grains such as samples C-1 and C-2, apparently averages out individual inhomogeneities. This effect leads to loss of valuable isotopic information stored in single mineral grains. Age interpretation based on samples C-1 and C-2 alone would have yielded just a minimum age of crystallization. The importance of a technique, permitting analysis of specially selected single grains such as sample C-3 in order to generate the required spread of the data points, is clearly illustrated by the present case.

6. Summary

The zircon population of the Cacciola granite displays rather unusual textural and chemical characteristics. While the level of total-rock U concentrations is not atypical of granitic rocks and conforms to measurements within the neighboring granitoids, the zircons have extremely high average U concentrations not found elsewhere in this accessory mineral. In the relatively coarse zircon grain-size fraction which was studied by electron microprobe, U is distributed at high levels of concentration (> 1 wt.%) throughout the grains. In spots the U concentration reaches extreme values of up to 10 wt.%. With regard to texture, the zircons are unusual as nearly all of the grains are intergrown with an assemblage of predominantly Th-bearing mineral phases such as allanite as well as apatite containing inclusions of Th-U phases. The zircons appear rather euhedral in polished sections and are generally mantled by the other mineral phases.

U-Pb isotopic data obtained on two zircon fractions of differing size and magnetic susceptibility, on one single zircon grain and on one single monazite grain are discordant and form a precise linear array yielding an upper intercept

age of 292 ± 9 m.y. In view of the absence of any detectable pre-Variscan radiogenic Pb component this age is interpreted as the time of emplacement for the Cacciola granite. It conforms with the less precise Rb-Sr total-rock age of the Rotondo granite. In view of the massive structure of the Rotondo and Cacciola granites and the more schistose structure of the closely associated Gamsboden and Fibbia gneisses, the age of the Cacciola granite can thus be regarded as a lower time limit for the tectonic activity which led to the overprint of this latter older group of granites. The lower intercept of 11 ± 9 m.y. is in good agreement with the age of a low grade, late Alpine phase of metamorphism which affected the area some 14 m.y. ago.

U-Pb systems of individual zircon grains show substantial variation. Such variation is essential for precise chronological interpretation of discordant data. It is prone, however, to be averaged out when fractions consisting of large numbers of grains are analyzed, as required by conventional techniques in order to generate data of sufficient quality. In the present case the ages obtained crucially depend on the precise analysis of the one single zircon crystal which provided the necessary spread of the data points.

The acid-leaching experiments performed on the samples indicate that substantial amounts of U, Th and Pb can be mobilized by such treatment which is often applied on a routine basis in the course of preparation of samples for isotope dilution analysis. Since these elements may become fractionated by differential leaching, an artificial «zero-age event» may be superimposed on preexisting discordance patterns, thus greatly reducing our ability to interpret such data. With the combination of electron microprobe and isotopic investigation, the U-Th-Pb systematics in the present case can be shown to be the direct result of the complex mineralogical properties of the samples. Th-rich phases intergrown with the zircon grains are easily attacked by the acid-treatment and consequently provide the bulk of the Th, U and Pb found in the leach solutions. It is conceivable that the presence of submicroscopic equivalents of such mineral phases which are easily overlooked, may at least be partially responsible for the complex U-Th-Pb data patterns observed in many zircon populations.

Acknowledgments

The help of Miss I. Bucher for mineral separation and of Mrs. H. Kälin for starting work in the rebuilt chemistry laboratory as well as for programming is gratefully acknowledged. We thank H. Baur, M. Décosterd, U. Derksen, E. Schärli and R. Schmid for technical support and Miss A. Reber for expert typing of the manuscript. We have benefitted from reviews by M. Casey, P. Signer and R. Wieler and from discussions with V. Köppel. The present analytical work would not have been possible without the ^{205}Pb spike generously supplied by G. J. Wasserburg. This study has been supported by grant 2.109-0.78 from the Swiss National Science Foundation.

Appendix I: The composition of common Pb

Since variable but significant amounts of ^{204}Pb are still present in all but one sample (C-3) after correction for analytical blank, a correction has to be made for the common Pb component incorporated by the samples during or subsequent to crystallization. The appropriate isotopic composition of this Pb phase has to be determinded either from direct measurement of minerals with low U/Pb and Th/Pb ratios such as feldspar or Pb ores, or by calculation on the basis of model assumptions. Considering the possibility of substantial redistribution of Pb during Alpine metamorphism the latter approach has been preferred. Using the model parameters of CUMMING and RICHARDS (1975, model III) and an age of 292 m.y. we obtain: $^{208}Pb/^{204}Pb = 38.30$, $^{207}Pb/^{204}Pb = 15.65$ and $^{206}Pb/^{204}Pb = 18.33$, which are the values used in Tables 3 and 4.

A plot of $^{207}Pb/^{204}Pb$ versus $^{206}Pb/^{204}Pb$ calculated from the data given in Table 4 (*S*- and *L*-fractions) yields an excellent linear array of the data points. Setting $^{206}Pb/^{204}Pb = 18.33$ (the value given above) a $^{207}Pb/^{206}Pb$ ratio of 15.60 ± 0.07 is obtained from this linear array which compares well with the ratio adopted from model parameters. This result therefore justifies the choice of the particular model Pb composition applied for the standard correction of the present samples.

Due to the low amount of common Pb contained in the single-zircon sample C-3, its data point is quite insensitive to shifts in the common Pb composition used for data reduction. For illustration the anomalous common Pb isotopic composition measured by GRÜNENFELDER and HAFNER (1962) in a K-feldspar from the Rotondo granite ($^{206}Pb/^{204}Pb = 19.51$, $^{207}Pb/^{204}Pb = 15.85$) was used for computation of the ages. The upper concordia intercept shifts to 300 m.y., still within limits of the age determined by use of model parameters. The lower intercept age on the other hand shifts to 35 m.y., governed by the data points of samples C-1 and C-2, which have relatively high contents of common Pb. It must be stressed however that the anomalous Pb composition used for this example does not conform with the Pb/Pb data array, which limits the maximum value for $^{207}Pb/^{204}Pb$ to 15.72, if $^{206}Pb/^{204}Pb$ is set to 19.51. We thus conclude that for all reasonable choices of a common Pb composition for correction, the uncertainty of the age of intrusion resulting from this correction is well within the range of $\pm$ 9 m.y. assigned to the upper concordia intercept age.

Appendix II: Th-U relationship

Although Th had not been measured by isotope dilution due to lack of facilities the U and Pb isotopic data provide some information on the Th content of the sample fractions analyzed. In the absence of fractionating loss or gain of lead between ^{232}Th-derived isotope ^{208}Pb and the ^{238}U-derived isotope ^{206}Pb, $^{232}Th/^{238}U$ ratios can be calculated on the basis of radiogenic $^{208}Pb/^{206}Pb$ ratios.

For the present case:

$$\frac{^{232}Th}{^{238}U} = K \frac{^{208}Pb}{^{206}Pb}$$

$$\text{where } K = \frac{e^{\lambda_{238}t}-1}{e^{\lambda_{232}t}-1} = 3.18,$$

t is the age of the samples (292 m.y.), λ_{238} and λ_{232} are the decay constants of ^{238}U and ^{232}Th, respectively. The apparent Th/U elemental ratios shown in Table 3 have been calculated under the assumption made above (non-fractionating loss of the two Pb isotopes). In complex natural systems such as those described here, this assumption will not be fulfilled. It is known that different mineral phases have different susceptibilities to Pb loss; there is a tendency that minerals primarily rich in

Th such as allanite, thorite and thorianite loose Pb at higher rates than for example the zircon phases. Nevertheless, the quite distinct trends of the data shown in Table 3 still allow for at least a qualitative discussion of the results.

The apparent Th/U ratios of the three leached zircon fractions (S-1, S-2 and S-3) vary from 0.13 to 0.22 and are within the range of the microprobe results (Table 1). Apparent Th/U ratios of the acid-leach fractions are considerably higher and appear to be dominated by sources rich in Th. According to literature data (cf. DEER et al., 1962) metamict allanite is soluble in hot concentrated HCl. The presence of the Th-U phases in apatite and of the Th-rich allanite both in intergrowth with the zircon fractions – as shown by the microprobe study (section 3.2) – thus easily explains the observed trend. Since most of the observed Th-bearing phases also contain appreciable amounts of U (Table 2) they do have a considerable influence on the U-Pb systems as illustrated by the present case (see section 5.3).

The unusually high $^{208}Pb/^{206}Pb$ ratio found for the accessory mineral grain S-A indicated that a Th-rich mineral and not a zircon had been analyzed. For lack of distinct morphology it had been included in the U-Pb analyses, because in our search for zircon grains with distinct properties its faint yellowish tint had set it apart from the majority of the zircon grains. The apparent Th/U ratio of the acid-leached sample S-A was exotic in comparison with the low Th/U ratios of the leached zircon samples. Its apparent Th content of 2.3 wt.% calculated from the data in Table 3 and its apparent Th/U ratio of 27 are compatible with the range of Th and U contents observed in monazite. We thus assume that sample S-A was a monazite. This problem of sample identification clearly demonstrates, that future analyses of unusual accessory minerals such as those encountered in this study will require grain-by-grain identification prior to analysis, for example by X-ray techniques.

References

AMBÜHL, E. (1929): Petrographie und Geologie des zentralen Gotthardmassivs südlich Andermatt. Schweiz. Min. Petr. Mitt. 9, 265–441.

ARMSTRONG, R. L. (1978): Pre-Cenozoic Phanerozoic Time Scale – Computer File of Critical Dates and Consequences of New and In-Progress Decay-Constant Revisions. In: Contrib. to the Geologic Time Scale (eds.: G. V. Cohee, M. F. Glaessner and H. D. Hedberg), 73–91. The American Association of Petroleum Geologists, Tulsa, Oklahoma, USA.

BURINGTON, R. S. and MAY, D. C., JR. (1970): Handbook of probability and statistics with tables. 2nd edition. McGraw-Hill, New York, 462 pp.

CHEN, J. H. and WASSERBURG, G. J. (1981): Isotopic Determination of Uranium in Picomole and Subpicomole Quantities. Analyt. Chem. 53, 2060–2067.

CUMMING, G. L. and RICHARDS, J. R. (1975): Ore Lead Isotope Ratios in a Continuously Changing Earth. Earth Planet. Sci. Lett. 28, 155–171.

DEER, W. A., HOWIE, R. A. and ZUSSMAN, J. (1962): Rock-Forming Minerals. Vol. 1. Ortho- and Ring Silicates. Longmans, London, 333 pp.

FREY, M., BUCHER, K., FRANK, E. and MULLIS, J. (1980): Alpine metamorphism along the Geotraverse Basel-Chiasso – a review. Eclogae geol. Helv. 73/2, 527–546.

GAUDETTE, H. E., VITRAC-MICHARD, A. and ALLÈGRE, C. J. (1981): North American Precambrian history recorded in a single sample: high-resolution U-Pb systematics of the Potsdam sandstone detrital zircons, New York State. Earth Planet. Sci. Lett. 54, 248–260.

GEBAUER, D. and GRÜNENFELDER, M. (1974): Rb-Sr Whole-Rock Dating of Late Diagenetic to Anchimetamorphic, Palaeozoic Sediments in Southern France (Montagne Noire). Contrib. Mineral. Petrol. 47, 113–130.

GOLDICH, S.S. and MUDREY, M.G., JR. (1972): Dilatancy model for discordant U-Pb zircon ages. Contrib. to Recent Geochemistry and Analytical Chemistry (A.P. Vinogradov Volume), Tugarinov A.I., ed., Moscow, Nauka Publ. Office, 415–418.

GRAUERT, B., GEBAUER, D. and SIGNER, P. (1973): Aufbau, Charakteristika und Messergebnisse eines automatisierten Tandem-Massenspektrometers (Abstract). Fortschr. Mineral. 50, Beiheft 3, 29.

GRÜNENFELDER, M. (1962): Mineralalter von Gesteinen aus dem Gotthardmassiv. Schweiz. Min. Petr. Mitt. 42, 6–7.

GRÜNENFELDER, M. and HAFNER, S. (1962): Über das Alter und die Entstehung des Rotondogranits. Schweiz. Min. Petr. Mitt. 42, 169–207.

GRÜNENFELDER, M. (1963): Heterogenität akzessorischer Zirkone und die petrogenetische Deutung ihrer Uran/Blei-Zerfallsalter. I. Der Zirkon des Granodioritgneises von Acquacalda (Lukmanierpass). Schweiz. Min. Petr. Mitt. 43, 235–257.

HAFNER, S. (1958): Petrographie des südwestlichen Gotthardmassivs (zwischen St.-Gotthardpass und Nufenenpass). Schweiz. Min. Petr. Mitt. 38, 255–362.

HAFNER, S., GÜNTHERT, A., BURCKHARDT, C.E., STEIGER, R.H., HANSEN, J.W. and NIGGLI, C.R. (1975): Geologischer Atlas der Schweiz 1:25000. Blatt 1251 Val Bedretto. Schweiz. Geol. Kommission.

HEIM, A. (1921): Geologie der Schweiz. Band 2: Die Schweizeralpen. Tauchnitz, Leipzig, 476 pp.

HOFMÄNNER, F.J. (1964): Petrographische Untersuchung der granitoiden Gesteine zwischen Gotthard- und Witenwasserenreuss. Dissertation Universität Zürich, 76 pp.

JAFFEY, A.H., FLYNN, K.F., GLENDENIN, L.E., BENTLEY, W.C. and ESSLING, A.M. (1971: Precision Measurements of Half-Lives and Specific Activities of ^{235}U and ^{238}U. Phys. Rev. C. 4, 1889–1906.

JÄGER, E. and NIGGLI, E. (1964): Rubidium-Strontium-Isotopenanalysen an Mineralien und Gesteinen des Rotondogranites und ihre geologische Interpretation. Schweiz. Min. Petr. Mitt. 44, 61–81.

JÄGER, E., NIGGLI, E., and WENK, E. (1967): Rb-Sr Altersbestimmungen an Glimmern der Zentralalpen. Beitr. Geol. Karte der Schweiz, Neue Folge, 134. Lieferung, 67 pp.

JÄGER, E. (1979): The Rb-Sr Method, in "Lectures in Isotope Geology", ed. E. Jäger and J.C. Hunziker, Springer Verlag, pp. 13–26.

KÖPPEL, V. and GRÜNENFELDER, M. (1971): A Study of Inherited and Newly Formed Zircons from Paragneisses and Granitised Sediments of the Strona-Ceneri-Zone (Southern Alps). Schweiz. Min. Petr. Mitt. 51, 385–409.

KÖPPEL, V. and SOMMERAUER, J. (1974): Trace Elements and the Behaviour of the U-Pb System in Inherited and Newly Formed Zircons. Contrib. Mineral. Petrol. 43, 71–82.

KROGH, T.E. (1973): A Low-Contamination Method for Hydrothermal Decomposition of Zircon and Extraction of U and Pb for Isotopic Age Determinations. Geochim. Cosmochim. Acta 37, 485–494.

KROGH, T.E. and DAVIS, G.L. (1975): Alteration in Zircons and Differential Dissolution of Altered and Metamict Zircon. Carnegie Institution of Washington Year Book 74, 619–623.

KVALE, A. (1957): Gefügestudien im Gotthardmassiv und den angrenzenden Gebieten. Schweiz. Min. Petr. Mitt. 37, 399–434.

LANCELOT, J., VITRAC, A. and ALLÈGRE, C.J. (1976): Uranium and lead isotopic dating with grain-by-grain zircon analysis: a study of complex geological history with a single rock. Earth Planet. Sci. Lett. 29, 357–366.

LUDWIG, K.R. and STUCKLESS, J.S. (1978): Uranium-Lead Isotope Systematics and Apparent Ages of Zircons and Other Minerals in Precambrian Granitic Rocks, Granite Mountains, Wyoming. Contrib. Mineral. Petrol. 65, 243–254.

LUDWIG, K.R. (1980): Calculation of Uncertainties of U-Pb Isotope Data. Earth Planet. Sci. Lett. 46, 212–220.

MATTINSON, J.M. (1972): Preparation of Hydrofluoric, Hydrochloric and Nitric Acids at Ultralow Lead Levels. Analyt. Chem. 44, 1715–1716.

MICHARD-VITRAC, A., LANCELOT, J., ALLÈGRE, C.J. and MOORBATH, S. (1977): U-Pb ages on single zircons from the early Precambrian rocks of west Greenland and the Minnesota River Valley. Earth Planet. Sci. Lett. 35, 449–453.

OBERLI, F. (1976): A U-Pb and Rb-Sr isotope study of a migmatite area, Scoresby Sund, East Greenland. Dissertation ETH Zürich.

RYBACH, L. and HAFNER, S. (1962): Radioaktivitätsmessungen an Gesteinen des St. Gotthard-Profils. Schweiz. Min. Petr. Mitt. 42, 209–219.

SCHÄRER, U. and ALLÈGRE, C.J. (1981 a): Investigation of the Precambrian crust by grain U-Pb analyses of detrital zircon (abstract). Terra Cognita, Journal of European Union of Geosciences, Special Issue, Spring 1981, 100–101.

SCHÄRER, U. and ALLÈGRE, C.J. (1981 b): U-Pb dating of domains of a single zircon grain (abstract). Terra Cognita, Journal of European Union of Geosciences, Special Issue, Spring 1981, 122.

SOMMERAUER, J. (1974): Trace element distribution patterns and the mineralogical stability of zircon – an application for combined electron microprobe techniques. Electron Microscopy Society of South. Africa, Proceedings 4, 71–72.

SOMMERAUER, J. (1976): Die chemisch-physikalische Stabilität natürlicher Zirkone und ihr U-(Th)-Pb System. Dissertation ETH Zürich, 151 pp.

SONDER, R.A. (1921): Untersuchungen über den Differentiationsverlauf der spätpaläozoischen Granitintrusionen im zentralen und westlichen Gotthardmassiv. Dissertation Universität Zürich, 71 pp.

STEIGER, R.H. and WASSERBURG, G.J. (1969): Comparative U-Th-Pb systematics in 2.7 x 10^9 yr plutons of different geologic histories. Geochim. Cosmochim. Acta 33, 1213–1232.

STEIGER, R.H. and JÄGER, E. (1977): Subcommission of Geochronology: Convention on the use of decay constants in geo- and cosmochronology. Earth Planet. Sci. Lett. 36, 359–362.

STEIGER, R.H. and BUCHER, I. (1978): Are Rb-Sr biotite ages in the Central Alps necessarily cooling ages? Short papers of the 4th Int. Conf. Geochronology, Cosmochronology, Isotope Geology. U.S. Geol. Survey Open-File Report 78-701, 414–415.

TERA, F. and WASSERBURG, G.J. (1975): Precise Isotopic Analysis of Lead in Picomole and Subpicomole Quantities. Analyt. Chem. 47, 2214–2220.

TILTON, G.R. (1960): Volume Diffusion as a Mechanism for Discordant Lead Ages. J. Geophys. Res. 65, 2933–2945.

TRÜMPY, R. (1980): Geology of Switzerland, a guide book. Ed.: Schweiz. Geol. Kommission. Wepf, Basel and New York, 334 pp.

WAGNER, G.A., REIMER, G.M. and JÄGER, E. (1977): Cooling Ages Derived by Apatite Fission-Track, Mica Rb-Sr and K-Ar Dating: The Uplift and Cooling History of the Central Alps. Memorie degli Istituti di Geologia e Mineralogia, Università di Padova, vol. 30, 1–27.

WASSERBURG, G.J. (1963): Diffusion Processes in Lead-Uranium Systems. J. Geophys. Res. 68, 4823–4846.

WASSERBURG, G.J., TERA, F., PAPANASTASSIOU, D.A. and HUNEKE, J.C. (1977): Isotopic and chemical investigations on Angra Dos Reis. Earth Planet. Sci. Lett. 35, 294–316.

WETHERILL, G.W. (1956): An interpretation of the Rhodesia and Witwatersrand age patterns. Geochim. Cosmochim. Acta 9, 290–292.

WILLIAMSON, J.H. (1968): Least-squares fitting of a straight line. Can. J. Phys. 46, 1845–1847.

YORK, D. (1969): Least Squares Fitting of a Straight Line With Correlated Errors. Earth Planet. Sci. Lett. 5, 320–324.

Manuscript received 31 october 1981